INTERNATIONAL JOURNAL FOR NUMERICAL METHODS IN BIOMEDICAL ENGINEERING
Int. J. Numer. Meth. Biomed. Engng. 2010; **26**:1404–1416
Published online 10 February 2009 in Wiley Online Library (wileyonlinelibrary.com). DOI: 10.1002/cnm.1221
COMMUNICATIONS IN NUMERICAL METHODS IN ENGINEERING

A simplified mesh-free method with embedded discontinuities

H. Wang and S. Wang*, †

Department of Engineering Mechanics, Tsinghua University, Beijing, China

SUMMARY

A simplified mesh-free method with embedded discontinuities is presented. In this method, the crack can be arbitrarily oriented, but its growth is represented discretely by activation of crack surfaces at individual particles, so no representation of the crack surface is needed. The crack is modeled by a local enrichment of the test and trial functions with a sign function, so that the discontinuities are along the direction of the crack. The discontinuity consists of cohesive crack segments that pass through the entire domain of influence at the node. A set of cracking rules is developed to avoid spurious cracking. We show by numerical experiments that complicated crack patterns with branching cracks can be modeled independent of the mesh. Copyright © 2009 John Wiley & Sons, Ltd.

Received 12 June 2008; Revised 30 November 2008; Accepted 1 December 2008

KEY WORDS: meshless; crack; cohesive segment; enrichment; fracture

1. INTRODUCTION

Besides the existence of numerous powerful computational methods for crack problems [1–9], the simulation of a large set of evolving cracks by computational methods still poses substantial difficulties. The most pertinent difficulty is tracking the crack path that becomes especially cumbersome for a large set of evolving cracks. Mesh-free methods are particularly suited for crack problems since they do not rely on a mesh that needs to be adjusted once a crack propagates. The visibility method [10–12] or improvements of the visibility method [13] are commonly used for problems involving cracks. Recently, level set methods have been used by some mesh-free methods for crack problems [14, 15]. Though no remeshing is needed in mesh-free methods, the need to track the crack path remains. Recently, mesh-free methods were developed that do not need to track the crack path [16–19]. In these methods, the crack is modeled by a set of cracked nodes. These can be arbitrarily oriented, but the growth is represented discretely by activation of crack surfaces at individual nodes, so no representation of the crack surface is needed. The crack is modeled by a local enrichment of the test and trial functions with a sign function, so that the discontinuities are along the direction of the crack. The discontinuity consists of cohesive crack segments that pass through the entire domain of influence at the node. One major advantage of the method is that it can handle crack propagation and crack nucleation in the same manner. However, the approach presented in [16] often leads to spurious cracking adjacent to existing crack and henceforth to an overestimation of the cohesive fracture energy similar to interface elements [2, 20]. Other recent mesh-free methods for fracture are given e.g. by [21–30].

We present a modification of the method in [16]. The major goal is to remove spurious cracking and simultaneously maintain the simplicity of the method. This is accomplished by defining a set

*Correspondence to: S. Wang, Department of Engineering Mechanics, Tsinghua University, Beijing, China.
†E-mail: s-wang@windowslive.com

of cracking rules. Since spurious cracking occurs only at crack propagation, crack propagation has to be distinguished from crack nucleation. In other words, the cracking rules presented later are only used for propagating cracks. We show by some numerical experiments that we are able to capture complicated crack patterns. We also show that we are able to avoid spurious cracking and get convergence in the cohesive fracture energy even for complicated crack problems.

The paper is outlined as follows: We first describe the element-free Galerkin (EFG) method and the new cracking method. Then, the discrete equations are derived from the weak form. The cracking criterion and the cohesive model are described next. At the end, we will show three examples before we conclude our paper.

2. EFG METHOD

The new cracking method is incorporated in a version of the EFG method [31]. The EFG method is based on the moving least-square approximation written in terms of a polynomial basis $\mathbf{p}(\mathbf{X})$ and unknown coefficients $\mathbf{a}(\mathbf{X})$:

$$\mathbf{u}^{\mathrm{con}}(\mathbf{X},t)=\sum_{I\in\mathscr{W}} p_I(\mathbf{X})a_I(\mathbf{X})=\mathbf{p}^{\mathrm{T}}(\mathbf{X})\mathbf{a}(\mathbf{X}) \tag{1}$$

where $\mathscr{W}$ is the total set of nodes; $\mathbf{p}^{\mathrm{T}}(\mathbf{X})=(1,X,Y)$. Minimization of discrete-weighted $\mathscr{L}_2$ error norm E with respect to the unknown coefficients $\mathbf{a}$

$$E=\sum_{I\in\mathscr{W}} (\mathbf{p}^{\mathrm{T}}(\mathbf{X}_I)\mathbf{a}(\mathbf{X}_I)-\mathbf{u}_I)^2 w(\mathbf{X}-\mathbf{X}_I,h) \tag{2}$$

leads to the final EFG approximation

$$\mathbf{u}^{\mathrm{con}}(\mathbf{X},t)=\sum_{I\in\mathscr{W}} N_I(\mathbf{X})\mathbf{u}_I(t) \tag{3}$$

with

$$N_I(\mathbf{X})=\mathbf{p}^{\mathrm{T}}(\mathbf{X})A^{-1}(\mathbf{X})\mathbf{D}_I(\mathbf{X}) \tag{4}$$

and

$$\begin{aligned}\mathbf{D}_I(\mathbf{X}) &= w(\mathbf{X}-\mathbf{X}_I,h)\mathbf{p}^{\mathrm{T}}(\mathbf{X}_I)\\ \mathbf{A}_I(\mathbf{X}) &= \sum_{I\in\mathscr{W}} w(\mathbf{X}-\mathbf{X}_I,h)\mathbf{p}(\mathbf{X}_I)\mathbf{p}^{\mathrm{T}}(\mathbf{X}_I)\end{aligned} \tag{5}$$

The superimposed con in Equation (3) denotes the continuous displacement field; $w(\mathbf{X}-\mathbf{X}_I,h)$ is the weighting function and h is the interpolation radius of this weighting function. For dynamic fracture, it is important to express the weighting function in terms of material coordinates since kernel functions expressed in spatial coordinates can lead to instabilities and numerical fracture as shown by e.g. [32, 33].

3. DISPLACEMENT FIELD

Consider a displacement field that is continuous in the entire domain except at the crack where a discontinuity occurs in the displacement field. To describe this discontinuity, the displacement is decomposed into continuous and discontinuous parts:

$$\mathbf{u}(\mathbf{X})=\underbrace{\mathbf{u}^{\mathrm{con}}(\mathbf{X})}_{\text{continuous}}+\underbrace{\mathbf{u}^{\mathrm{dis}}(\mathbf{X})}_{\text{discontinuous}} \tag{6}$$

In [16], the crack is modeled by a set of discrete cracks that cross the entire domain of influence of a node. These discrete cracks are restricted to lie on a plane passing through this node, see Figure 1. The major advantage is that no representation for the geometry of the crack is needed.

DOI: 10.1002/cnm

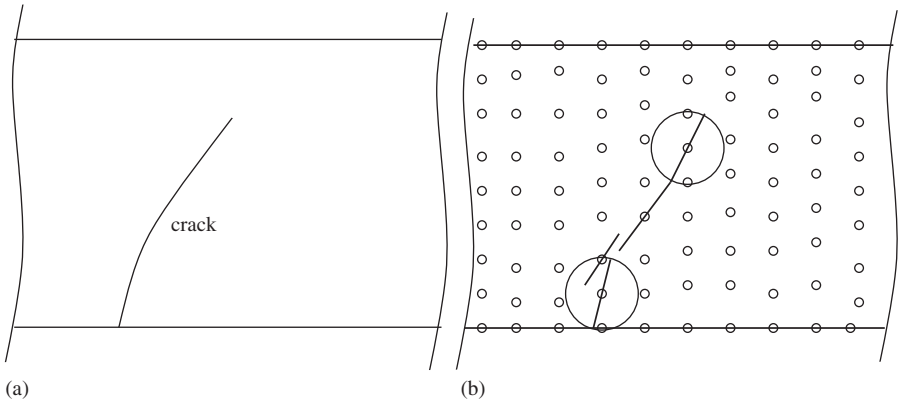

Figure 1. (a) Continuous crack and (b) representation of the crack with discrete cohesive crack segments.

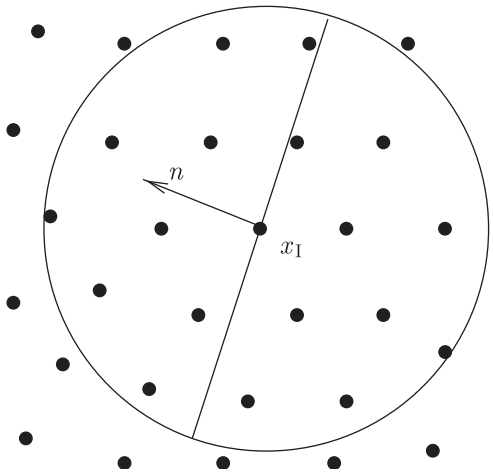

Figure 2. Normal of the crack segment.

The approximation of the discontinuous displacement field is

$$\mathbf{u}^{\mathrm{dis}}(\mathbf{X}) = \sum_{I \in \mathscr{W}_{\mathrm{c}}} N_I(\mathbf{X}) H(\mathbf{X}) \mathbf{q}_I \tag{7}$$

where $\mathscr{W}_{\mathrm{c}}$ is the set of cracked nodes, $\mathbf{q}_I$ are additional unknowns and $H(\mathbf{X})$ is the step function that introduces the jump in the displacement field. Note that only cracked nodes are enriched that significantly simplify the implementation of the method. Only a small portion of the entire nodes are affected by the crack and the crack surface is entirely determined by the position vector of the cracked node and its normal that is obtained from the cracking criterion explained later, Figure 2:

$$H(\mathbf{X}) = \begin{cases} 1 & \text{if } \mathbf{n} \cdot (\mathbf{X} - \mathbf{X}_I) > 0 \\ -1 & \text{if } \mathbf{n} \cdot (\mathbf{X} - \mathbf{X}_I) < 0 \end{cases} \tag{8}$$

The crack normal in the initial configuration is obtained by Nanson's law. The jump in the displacement field only depends on the additional unknowns $\mathbf{q}$ and is given by

$$[[\mathbf{u}]](\mathbf{X}) = \sum_{I \in \mathscr{W}_{\mathrm{c}}} 2 N_I(\mathbf{X}) \mathbf{q}_I \tag{9}$$

DOI: 10.1002/cnm

The test functions $\delta\mathbf{u}$ have a similar structure:

$$\delta\mathbf{u}(\mathbf{X}) = \sum_{I\in\mathscr{W}} N_I(\mathbf{X})\delta\mathbf{u}_I(t) + \sum_{I\in\mathscr{W}_c} N_I(\mathbf{X})H(\mathbf{X})\delta\mathbf{q}_I \tag{10}$$

Note that we use the same shape functions and same domain of influence for continuous and discontinuous displacement field.

As noted in the introduction, without further modification of the method, spurious crack nucleation is obtained when the crack propagates. This will be demonstrated later for some numerical examples. Therefore, we suggest the following modifications:

- A criterion is needed that distinguishes crack nucleation from crack propagation.
- A criterion is needed for crack branching.
- A criterion is needed to avoid spurious cracking.

Crack nucleation is distinguished from crack propagation by searching for existing cracked nodes in the vicinity of a newly inserted cracked node. The search domain is a circle of radius αr_m with r_m being the interpolation radius of the weighting function and α is a parameter. In all computations, the parameter α is set to 1.2 though results did not significantly change for any $1.2 < \alpha < 2.0$.

Spurious cracking can occur adjacent to an existing crack, Figure 3, or close to the crack tip, Figure 4. The first type of spurious cracking is avoided by an exclusion zone that does not allow development of *parallel* cracks far away from the crack tip, Figure 3. The crack tip is defined as the last cracked node for the case 'crack propagation'.

In most dynamic computations, cracking criterion is met at several material points around the crack tip due to similar stress states, Figure 3. This can lead to branching cracks. Allowing only one node in front of the crack tip to crack avoids crack branching completely. Therefore, a criterion for crack branching has to be introduced first. A crack is assumed to branch if the angle between an existing crack tip node and newly initiated cracks exceeds a certain value. Therefore, we compute

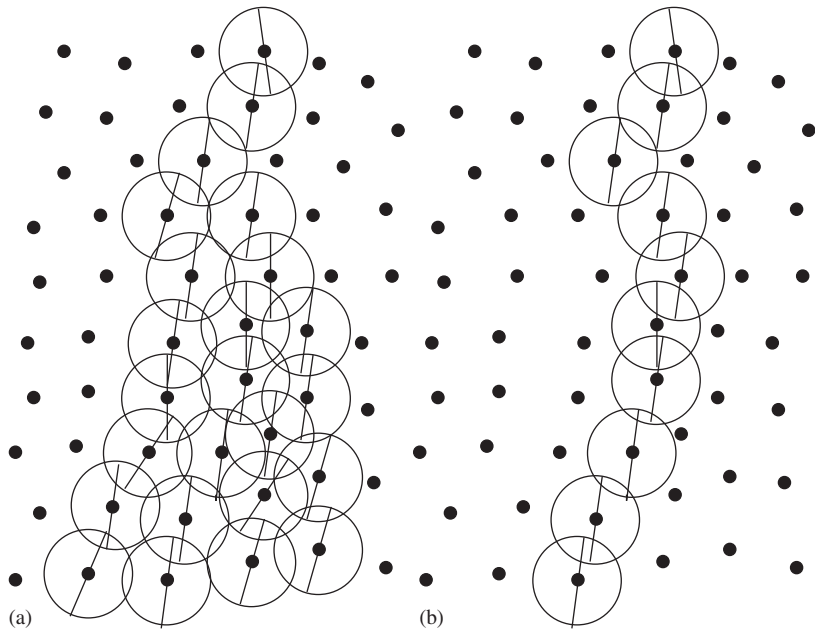

Figure 3. (a) Spurious cracking during crack propagation and (b) crack propagation without spurious cracking.

DOI: 10.1002/cnm

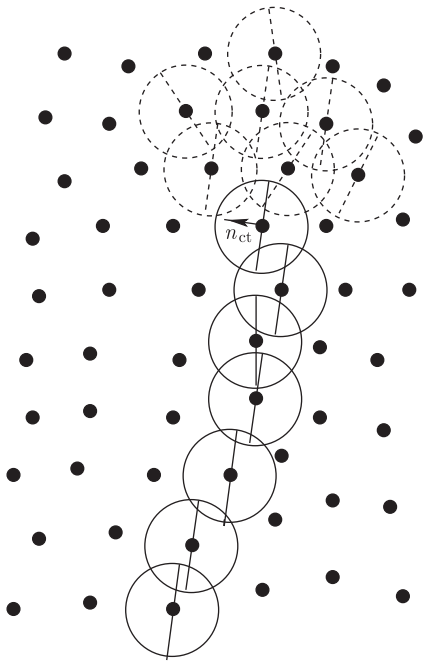

Figure 4. Crack with crack tip node (solid line) at time n and nodes that meet cracking criterion at time $n+1$ (dashed line).

deviation in the crack direction, Figure 4:

$$\gamma_{\max} = \underbrace{\max}_{I \in \tilde{\mathscr{W}}_c} (\mathbf{n}_{ct} \cdot \mathbf{n}_I) \quad \forall I \in \tilde{\mathscr{W}}_c \tag{11}$$

$$\gamma_{\min} = \underbrace{\min}_{I \in \tilde{\mathscr{W}}_c} (\mathbf{n}_{ct} \cdot \mathbf{n}_I) \quad \forall I \in \tilde{\mathscr{W}}_c \tag{12}$$

where $\tilde{\mathscr{W}}_c \subset \mathscr{W}_c$ is the set of newly cracked nodes, i.e. between time step n and time step $n+1$. If $\gamma_{\max} - \gamma_{\min} \geqslant$ TOL, the crack branches. In the current implementation, we allow only two branches though this is not compulsory.

After deciding if crack branches or not, a criterion has to be implemented that avoids spurious cracking. Let $K = 1$ or 2 denote the number of crack branches of an associated advancing crack. Then, K number of cracked nodes are introduced in front of an existing crack tip. The closest node(s) where the cracking criterion is met will be cracked. If $K = 2$, two crack tips (of the original 1 crack) will exist in the next time step.

It is instructive to mention that generally cracking criterion is met at several material points under crack initiation. In this case, we also allow only one node to crack at a time. The position of the cracked node is obtained by an average procedure. The closest node to the averaged position vector of all nodes that meets cracking criterion is cracked.

4. WEAK FORM AND DISCRETIZATION

The linear momentum equation is

$$\nabla \cdot \mathbf{P} + \varrho \mathbf{b} = \varrho \ddot{\mathbf{u}}, \quad \mathbf{X} \in \Omega \tag{13}$$

DOI: 10.1002/cnm

where $\mathbf{P}$ is the nominal stress tensor, ϱ is the density, $\mathbf{b}$ are body forces and the superimposed dots denote material time derivatives. The displacement and traction boundary conditions are

$$\mathbf{u} = \bar{\mathbf{u}}, \quad \mathbf{X} \in \Gamma_u \tag{14}$$

$$\mathbf{n}_t \cdot \mathbf{P} = \bar{\mathbf{t}}, \quad \mathbf{X} \in \Gamma_t \tag{15}$$

$$\mathbf{n}_c \cdot \mathbf{P} = \mathbf{t}_c([[\mathbf{u}]]), \quad \mathbf{X} \in \Gamma_c \tag{16}$$

where the index c refers to the crack, the index t refers to traction boundaries and the index u refers to displacement boundaries. The weak form of the linear momentum equation is: Find $\mathbf{u} \in \mathscr{U}$ and $\delta\mathbf{u} \in \mathscr{U}_0$ such that

$$\delta W = \delta W_{\text{int}} - \delta W_{\text{ext}} + \delta W_{\text{inertia}} + \delta W_{\text{coh}} = 0 \tag{17}$$

with

$$\begin{aligned} \delta W_{\text{int}} &= \int_\Omega \nabla\delta\mathbf{u} : \mathbf{P}\, d\Omega \\ \delta W_{\text{ext}} &= \int_{\Gamma_t} \delta\mathbf{u} \cdot \bar{\mathbf{t}}\, d\Gamma + \int_\Omega \varrho\delta\mathbf{u} \cdot \mathbf{b}\, d\Omega \\ \delta W_{\text{inertia}} &= \int_\Omega \varrho\delta\mathbf{u} \cdot \ddot{\mathbf{u}}\, d\Omega \\ \delta W_{\text{coh}} &= \int_{\Gamma_c} \delta[[\mathbf{u}]] \cdot \mathbf{t}_c\, d\Gamma \end{aligned} \tag{18}$$

and $\mathscr{U}$ and $\mathscr{U}_0$ are the approximation spaces for the trial and test functions:

$$\begin{aligned} \mathscr{U} &= \{\mathbf{u}(\mathbf{X}, t) | \mathbf{u} \in H^1,\ \mathbf{u} = \bar{\mathbf{u}} \text{ on } \Gamma_u,\ \mathbf{u} \text{ discontinuous on } \Gamma_c\} \\ \mathscr{U}_0 &= \{\delta\mathbf{u} | \delta\mathbf{u} \in H^1,\ \delta\mathbf{u} = 0 \text{ on } \Gamma_u,\ \delta\mathbf{u} \text{ discontinuous on } \Gamma_c\} \end{aligned} \tag{19}$$

The discretized equations are obtained by substituting the test and trial functions into Equation (17):

$$\sum_{J=1}^{n} \int_{\Omega_J} \nabla\delta\mathbf{u}_J : \mathbf{P}\, d\Omega - \sum_{J=1}^{n} \int_{\Gamma_{t,J}} \delta\mathbf{u} \cdot \bar{\mathbf{t}}\, d\Gamma - \sum_{J=1}^{n} \int_{\Omega_J} \varrho\delta\mathbf{u} \cdot \mathbf{b}\, d\Omega$$

$$+ \int_{\Gamma_{c,J}} \delta[[\mathbf{u}]] \cdot \mathbf{t}_c\, d\Gamma + \sum_{J=1}^{n} \int_{\Omega_J} \varrho\delta\mathbf{u} \cdot \ddot{\mathbf{u}}\, d\Omega = 0 \tag{20}$$

The final system of equations in matrix form is given by

$$\begin{bmatrix} \mathbf{M}_{IJ}^{uu} & \mathbf{M}_{IJ}^{uq} \\ \mathbf{M}_{IJ}^{qu} & \mathbf{M}_{IJ}^{qq} \end{bmatrix} \cdot \begin{bmatrix} \ddot{\mathbf{u}}_J \\ \ddot{\mathbf{q}}_J \end{bmatrix} = \begin{bmatrix} \mathbf{f}_{I,\text{ext}}^{u} - \mathbf{f}_{I,\text{int}}^{u} \\ \mathbf{f}_{I,\text{ext}}^{q} - \mathbf{f}_{I,\text{int}}^{q} \end{bmatrix} \tag{21}$$

with

$$\mathbf{f}_{I,\text{ext}}^{u} = \int_{\Gamma_t} (\mathbf{N}_I^u)^{\mathrm{T}}\, \mathbf{t}\, d\Gamma + \int_\Omega (\mathbf{N}_I^u)^{\mathrm{T}} \mathbf{b}\, d\Omega \tag{22}$$

$$\begin{aligned} \mathbf{f}_{I,\text{ext}}^{q} = &\int_{\Gamma_t} (\mathbf{N}_I^q)^{\mathrm{T}} \mathbf{t}\, d\Gamma + \int_\Omega (\mathbf{N}_I^q)^{\mathrm{T}} \mathbf{b}\, d\Omega \\ &+ \int_{\Gamma_c} [[(\mathbf{N}_I^q)^{\mathrm{T}}]]\, \mathbf{t}_c\, d\Gamma \quad \text{with } \mathbf{N}_I^q = \mathbf{N}_I \Psi(\mathbf{X}) \end{aligned} \tag{23}$$

$$\mathbf{f}_{I,\text{int}}^{u} = \int_\Omega (\mathbf{B}_I^u)^{\mathrm{T}} \mathbf{P}\, d\Omega \tag{24}$$

DOI: 10.1002/cnm

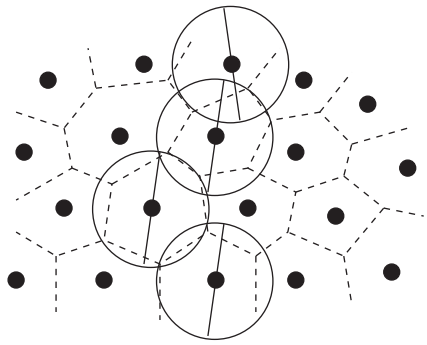

Figure 5. Cracked nodes with crack segments (solid line) and Voronoi cells (dashed line).

$$\mathbf{f}^q_{I,\text{int}} = \int_\Omega (\mathbf{B}^q_I)^{\mathrm{T}} \mathbf{P}\, \mathrm{d}\Omega \quad \text{with } \mathbf{B}^q_I = \Psi(\mathbf{X}) \nabla \mathbf{N}_I \tag{25}$$

$$\begin{aligned} \mathbf{M}^{uu}_{IJ} &= \mathbf{M}^{qq}_{IJ} = \int_\Omega \varrho \mathbf{N}_I \ \mathbf{N}^{\mathrm{T}}_J \, \mathrm{d}\Omega \\ \mathbf{M}^{uq}_{IJ} &= \mathbf{M}^{qu}_{IJ} = \int_\Omega \varrho \Psi(\mathbf{X}) \ \mathbf{N}_I \ \mathbf{N}^{\mathrm{T}}_J \, \mathrm{d}\Omega \end{aligned} \tag{26}$$

The integrals are evaluated by stress point integration as explained detailed in [16]. We use explicit central difference time integration. To benefit from explicit time integration, one generally takes advantage of lumped mass matrix. However, in the presence of additional degrees of freedom $\mathbf{q}$, standard mass lumping might lead to negative masses.

Cueto *et al.* [34] showed that the lumped mass matrix obtained via the volume of Voronoi cells ($M = V \cdot \varrho$, where V is the volume of the Voronoi cell and ϱ is the density of the material) is identical to lumped mass matrix from standard row-sum technique. We therefore build the lumped mass matrix from Voronoi cells. The mass of the (enriched) cracked node is modified according to its area ratio, Figure 5. Results by this method were similar to the results obtained from using consistent mass matrix. Since the cracked node always lies in the middle of the associated Voronoi cell, Figure 5, the critical time step is influenced only marginal. We use a Courant number of 0.5 and did not observe any instabilities.

5. CRACKING CRITERION AND COHESIVE LAW

Rankine criterion determines the onset of cracking and crack propagation. The crack is introduced perpendicular to the direction of the maximum principal stress. The traction acting across the crack surface is related to the jump in the displacement, Equation (9). It can be decomposed into a normal and tangential part:

$$\delta_{\mathrm{n}} = [[\mathbf{u}]] \cdot \mathbf{n} \tag{27}$$

$$\delta_{\mathrm{t}} = |[[\mathbf{u}]]_{\mathrm{s}} = |[[\mathbf{u}]] - \delta_{\mathrm{n}} \mathbf{n}| \tag{28}$$

We use the cohesive law proposed by Pandolfi *et al.* [35] that makes use of effective crack opening displacement

$$\delta = \sqrt{\beta^2 \delta^2_{\mathrm{t}} - \delta^2_{\mathrm{n}}} \tag{29}$$

DOI: 10.1002/cnm

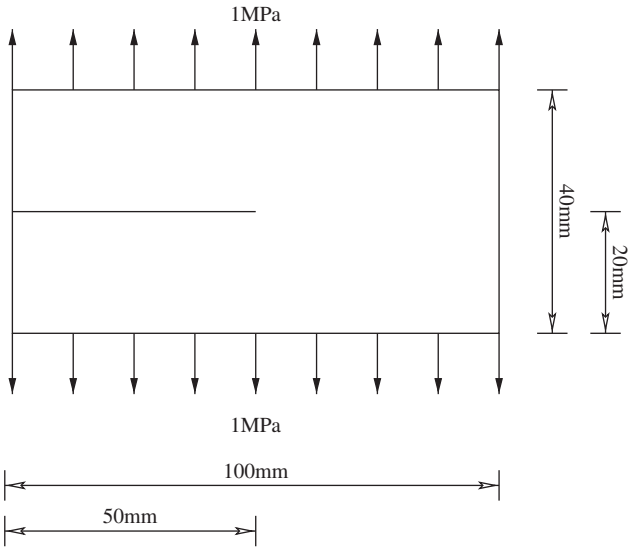

Figure 6. Plate with a horizontal initial notch under tensile tractions.

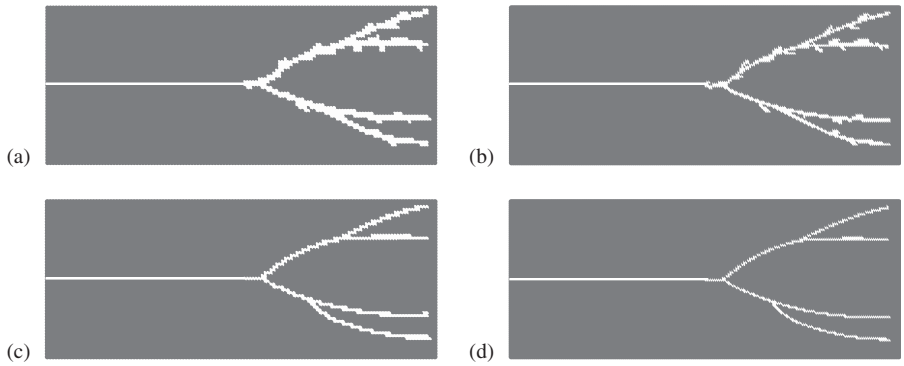

Figure 7. Crack pattern for the crack branching problem: (a) 4141 nodes, with spurious cracking; (b) 16 281 nodes, with spurious cracking; (c) 4141 nodes, without spurious cracking; and (d) 16 281 nodes, without spurious cracking.

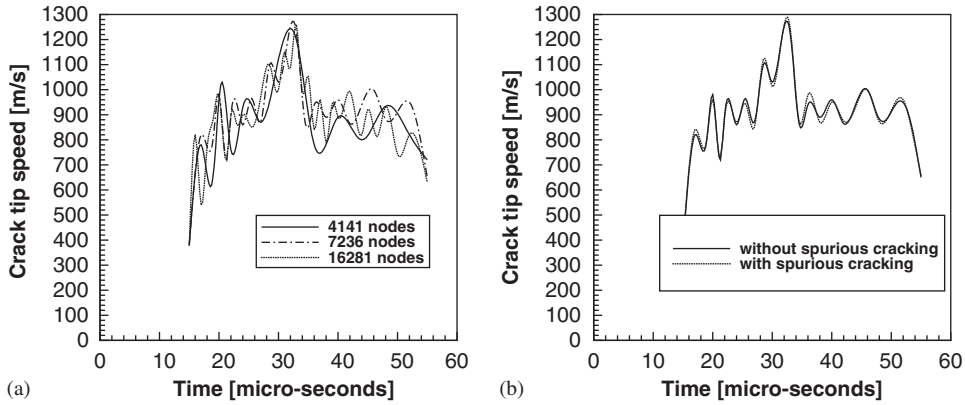

Figure 8. Crack tip speed for the crack branching problem: (a) without spurious cracking and (b) comparison with and without spurious cracking.

DOI: 10.1002/cnm

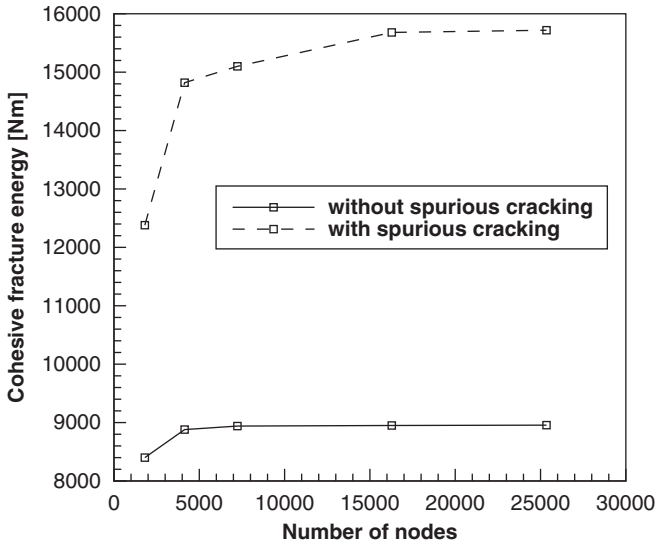

Figure 9. Cohesive fracture energy of the branching crack problem.

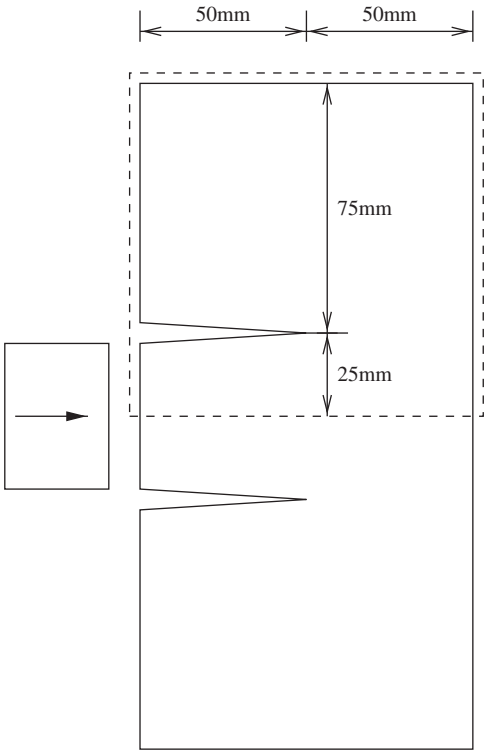

Figure 10. Kalthoff problem.

where the parameter β defines the ratio between tangential and normal critical traction. The effective traction-separation law is given by

$$t = \frac{t_{\max}}{\delta_{\max}}\delta \quad \text{if } \delta \leqslant \delta_{\max} \text{ or } \dot{\delta} < 0 \tag{30}$$

DOI: 10.1002/cnm

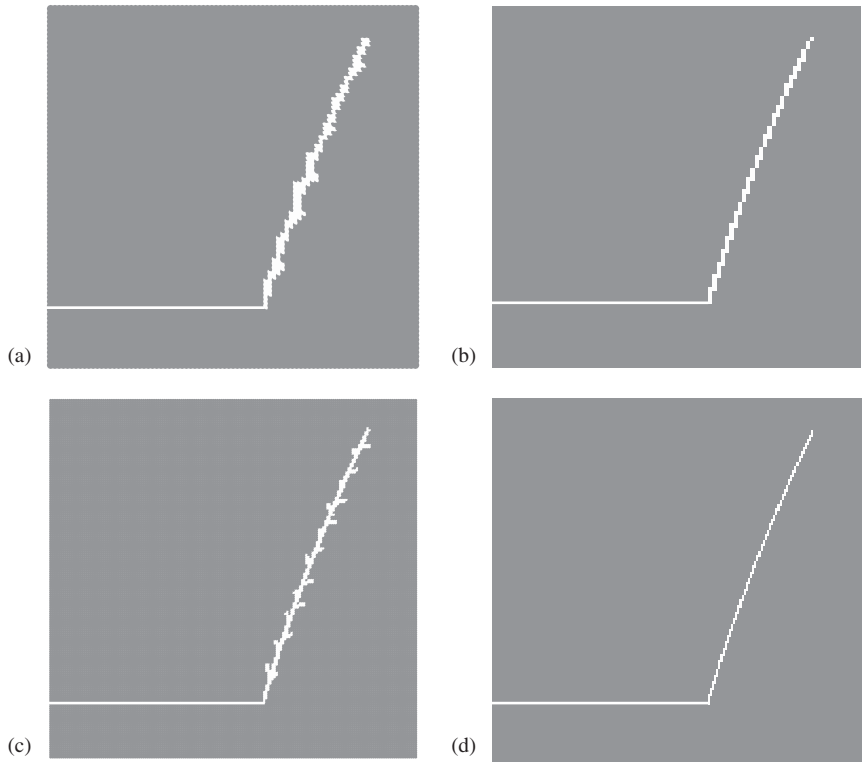

Figure 11. Final crack path of the Kalthoff problem: (a) 10 201 nodes, with spurious cracking; (b) 10 201 nodes, without spurious cracking; (c) 40 804 nodes, with spurious cracking; and (d) 40 804 nodes, without spurious cracking.

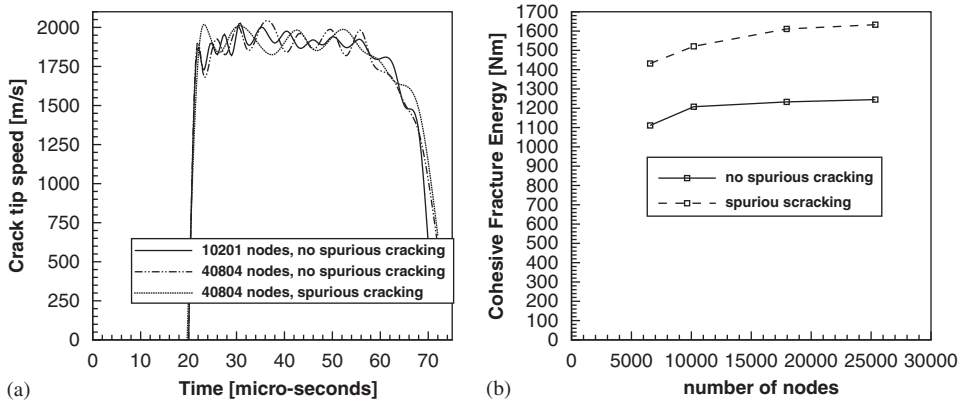

Figure 12. Crack tip speed and cohesive fracture energy of the Kalthoff problem: (a) crack tip speed and (b) cohesive fracture energy.

The traction vector is then computed by

$$\mathbf{t} = \frac{t}{\delta}(\beta^2[[\mathbf{u}]]_{\mathrm{s}} + \delta_{\mathrm{n}}\mathbf{n}) \tag{31}$$

More details are given in [35].

DOI: 10.1002/cnm

6. RESULTS

6.1. Crack branching

The first example is the pre-notched specimen under tensile loading, $\sigma = 1\,\text{MPa}$, shown in Figure 6. Numerical results for this problem are reported in [16, 20, 36] and experimental results with different dimensions are available in [37–39]. Young's modulus is $E = 32\,000\,\text{MPa}$ and Poisson's ratio is $\nu = 0.20$. The initial Rayleigh wave speed is $c_R = 2119.0\,\text{m/s}$. This problem is studied with different refinements. The tolerance angle deciding about crack branching was 30°. We also studied this problem without the set of cracking rules proposed in the previous sections.

The pattern of crack propagation at different stages of the simulation is shown in Figure 7. Without avoiding spurious cracking, the crack pattern is fringy and the width of the crack varies. These observations agree with the results in [16]. The speed of the crack tip is shown in Figure 8. The spurious cracks do not seem to have any influence on the crack speed. This suggests that the spurious cracks occur adjacent to the crack far away from the crack tip. We also observe increase in the crack speed before the crack branches. Afterwards, the crack speed decreases. This is in agreement with results reported by other authors [37–39].

The cohesive fracture energy is reported in Figure 9. It is lower when spurious cracking is avoided. The cohesive fracture energy diverges or converges very slowly when spurious cracking is not suppressed.

6.2. The Kalthoff experiment

Kalthoff and Winkler [40] reported experimental results in which a plate with two initial edge notches is impacted by a projectile. The experimental set-up is shown in Figure 10. The impact velocity is $20\,\text{m/s}$. In the experiment, a crack propagated with angle of about 70° versus the horizontal axis. We study this problem. Only the upper part of the plate is modeled due to symmetry. The material properties of the steel used in the experiment [41] are Young's modulus $E = 190\,\text{GPa}$, density $\varrho = 8000\,\text{kg/m}^3$ and Poisson's ratio $\nu = 0.3$. The crack path at the end of the simulation is illustrated in Figure 11 and agrees well with the experimental results. The crack speed is shown in Figure 12(a). It is not influenced by spurious cracking. However, the cohesive fracture energy is significantly higher when spurious cracking is not suppressed, Figure 12.

7. CONCLUSIONS

We presented a set of cracking rules to avoid spurious cracking in a simplified meshless method with embedded discontinuities. The simplified method is based on local partition of unity and introduces discrete cracks at nodes. The crack is represented by a set of discrete cracked nodes. No representation of crack surface is needed that makes the method appealing for many cracks.

We showed that the method can handle complicated problems with many cracks and also branching cracks. We showed improvements in the crack pattern and showed that with the cracking rules, convergence in the cohesive fracture energy is obtained.

REFERENCES

1. Li S, Simkins DC. Conserving Galerkin weak formulations for computational fracture mechanics. *Communications in Numerical Methods in Engineering* 2002; **18**:835–850.
2. Ortiz M, Leroy Y, Needleman A. Finite element method for localized failure analysis. *Computer Methods in Applied Mechanics and Engineering* 1987; **61**:189–213.
3. Belytschko T, Lu YY. Element-free Galerkin methods for static and dynamic fracture. *International Journal of Solids and Structures* 1995; **32**:2547–2570.
4. Belytschko T, Lu YY, Gu L. Crack propagation by element-free Galerkin methods. *Engineering Fracture Mechanics* 1995; **51**(2):295–315.
5. Bellec J, Dolbow JE. A note on enrichment functions for modelling crack nucleation. *Communications in Numerical Methods in Engineering* 2003; **19**(12):921–932.

DOI: 10.1002/cnm

6. Belytschko T, Tabbara M. Dynamic fracture using element-free Galerkin methods. *International Journal for Numerical Methods in Engineering* 1996; **39**(6):923–938.
7. Bordas S, Rabczuk T, Zi G. Three-dimensional crack initiation, propagation, branching and junction in non-linear materials by an extended meshfree method without asymptotic enrichment. *Engineering Fracture Mechanics* 2008; **75**(5):943–960.
8. Hao S, Liu WK, Klein PA, Rosakis AJ. Modeling and simulation of intersonic crack growth. *International Journal of Solids and Structures* 2004; **41**(7):1773–1799.
9. Volokh KY. Comparison between cohesive zone models. *Communications in Numerical Methods in Engineering* 2004; **20**(11):845–856.
10. Hao S, Liu WK, Chang CT. Computer implementation of damage models by finite element and meshfree methods. *Computer Methods in Applied Mechanics and Engineering* 2000; **187**:401–440.
11. Belytschko T, Lu YY, Gu L. Crack propagation by element-free Galkerin methods. *Engineering Fracture Mechanics* 1994; **51**:295–315.
12. Hao S, Liu WK, Weertman J. Cohesive solutions of intersonic moving dislocations. *Philisophical Magazine* 2004; **84**:1067–1104.
13. Organ D, Fleming M, Terry T, Belytschko T. Continuous meshless approximations for nonconvex bodies by diffraction and transparency. *Computational Mechanics* 1996; **18**:225–235.
14. Rabczuk T, Zi G. A meshfree method based on the local partition of unity for cohesive cracks. *Computational Mechanics* 2007; **39**(6):743–760.
15. Ventura G, Xu J, Belytschko T. A vector level set method and new discontinuity approximation for crack growth by EfG. *International Journal for Numerical Methods in Engineering* 2002; **54**(6):923–944.
16. Rabczuk T, Belytschko T. Cracking particles: a simplified meshfree method for arbitrary evolving cracks. *International Journal for Numerical Methods in Engineering* 2004; **61**(13):2316–2343.
17. Rabczuk T, Belytschko T. A three dimensional large deformation meshfree method for arbitrary evolving cracks. *Computer Methods in Applied Mechanics and Engineering* 2007; **196**:2777–2799.
18. Rabczuk T, Areias PMA, Belytschko T. A simplified mesh-free method for shear bands with cohesive surfaces. *International Journal for Numerical Methods in Engineering* 2007; **69**(5):993–1021.
19. Rabczuk T, Areias PMA, Belytschko T. A meshfree thin shell method for non-linear dynamic fracture. *International Journal for Numerical Methods in Engineering* 2007; **72**(5):524–548.
20. Xu XP, Needleman A. Numerical simulations of fast crack growth in brittle solids. *Journal of the Mechanics and Physics of Solids* 1994; **42**:1397–1434.
21. Hao S, Liu WK. Moving particle finite element method with superconvergence: nodal integration formulation and applications. *Computer Methods in Applied Mechanics and Engineering* 2006; **195**:6059–6072.
22. Hao S, Liu WK, Belytschko T. Moving particle finite element method with global smoothness. *International Journal for Numerical Methods in Engineering* 2004; **59**:1007–1020.
23. Hao S, Liu WK, Moran B, Olson GB. A hierarchical multi-physics model for design of high toughness steels. *Journal of Computer-Aided Materials Design* 2003; **10**:99–142.
24. Zhang GY, Liu GR, Wang YY, Huang HT, Zhong ZH, Li GY, Han X. A linearly conforming point interpolation method (LC-PIM) for three-dimensional elasticity problems. *International Journal for Numerical Methods in Engineering* 2007; **72**:1524–1543.
25. Rabczuk T, Zi G, Bordas S, Nguyen-Xuan H. A geometrically non-linear three dimensional cohesive crack method for reinforced concrete structures. *Engineering Fracture Mechanics* 2008; **75**:4740–4758.
26. Yoo JW, Moran B, Chen JS. Stabilized conforming nodal integration in the natural-element method. *International Journal for Numerical Methods in Engineering* 2004; **60**:861–890.
27. Hao S, Liu WK, Moran B, Vernerey F, Olson GB. Multi-scale constitutive model and computational framework for the design of ultra-high strength, high toughness steels. *Computer Methods in Applied Mechanics and Engineering* 2004; **193**:1865–1908.
28. Sze KY, Chen JS, Sheng N, Liu XH. Stabilized conforming nodal integration: exactness and variational justification. *Finite Elements in Analysis and Design* 2004; **41**:147–171.
29. Rabczuk T, Belytschko T. Adaptivity for structured meshfree particle methods in 2D and 3D. *International Journal for Numerical Methods in Engineering* 2005; **63**(11):1559–1582.
30. Hao S, Liu WK. Bimaterial interfacial crack growth with strain gradient theory. *Journal of Engineering Materials and Technology—Transactions of the ASME* 1999; **121**:413–421.
31. Belytschko T, Lu YY, Gu L. Element-free Galerkin methods. *International Journal for Numerical Methods in Engineering* 1994; **37**:229–256.
32. Belytschko T, Guo Y, Liu WK, Xiao SP. A unified stability analysis of meshfree particle methods. *International Journal for Numerical Methods in Engineering* 2000; **48**:1359–1400.
33. Rabczuk T, Belytschko T, Xiao SP. Stable particle methods based on Lagrangian kernels. *Computer Methods in Applied Mechanics and Engineering* 2004; **193**:1035–1063.
34. Cueto FL, Colominas I, Mosqueira G, Navarrina F, Casteleiro M. On the Galerkin formulation of smoothed particle hydrodynamics. *International Journal for Numerical Methods in Engineering* 2004; **60**:1475–1512.
35. Pandolfi A, Krysl P, Ortiz M. Finite element simulation of ring expansion and fragmentation: the capturing of length and time scales through cohesive models of fracture. *International Journal of Fracture* 1999; **95**:279–297.
36. Song J-H, Areais PMA, Belytschko T. A method for dynamic crack and shear band propagation with phantom nodes. *International Journal for Numerical Methods in Engineering* 2006; **67**:868–893.

DOI: 10.1002/cnm

37. Ravi-Chandar K. Dynamic fracture of nominally brittle materials. *International Journal of Fracture* 1998; **90**:83–102.
38. Sharon E, Gross PSP, Fineberg J. Local crack branching as a mechanism for instability in dynamic fracture. *Physical Review Letters* 1995; **74**:5096–5099.
39. Fineberg J, Sharon E, Cohen G. Crack front waves in dynamic fracture. *International Journal of Fracture* 2003; **121**:55–69.
40. Kalthoff JF, Winkler S. Failure mode transition at high rates of shear loading. *International Conference on Impact Loading and Dynamic Behavior of Materials* 1987; **1**:185–195.
41. Kalthoff JF. Modes of dynamic shear failure in solids. *International Journal of Fracture* 2000; **101**:1–31.

DOI: 10.1002/cnm